PHYSICAL REVIEW D **87,** 115020 (2013)

Anomaly mediated supersymmetric models and Higgs data from the LHC

Alexandre Arbey,[1,2,3,*] Aldo Deandrea,[2,†] Farvah Mahmoudi,[3,4,‡] and Ahmad Tarhini[2,§]

[1]*CRAL, Observatoire de Lyon, CNRS, UMR5574, 9 avenue Charles André, F-69561 Saint-Genis Laval Cedex, France and Ecole Normale Supérieure de Lyon, 46 allée d'Italie, F-69007 Lyon, France*

[2]*Université de Lyon, France and Université Lyon 1, CNRS/IN2P3, UMR5822 IPNL, F-69622 Villeurbanne Cedex, France*

[3]*Physics Department, CERN Theory Division, CH-1211 Geneva 23, Switzerland*

[4]*Clermont Université, Université Blaise Pascal, CNRS/IN2P3, LPC, BP 10448, F-63000 Clermont-Ferrand, France*

(Received 7 April 2013; published 18 June 2013)

Anomaly mediation models are well-motivated supersymmetry-breaking scenarios which appear as alternatives to the minimal supergravity paradigm. These models are quite compelling from the theoretical point of view and it is therefore important to test if they are also viable models for phenomenology. We perform a study of these models in the light of all standard flavor, collider and dark matter constraints, including also the recent Higgs boson measurements for the mass and signal strengths in the different decay channels. The minimal anomaly-mediated supersymmetry breaking (AMSB) scenario can satisfy in part of its parameter space the dark matter requirement but is only marginally consistent with the current Higgs boson mass value. The hypercharge-AMSB and mixed moduli-AMSB scenarios can better describe present data from dark matter, flavor, and low-energy physics and are consistent with the measured mass of the Higgs boson. The inclusion of the preferred signal strengths for the Higgs boson decay channels shows that for $\tan\beta \gtrsim 5$ the hypercharge-AMSB and mixed moduli-AMSB models can be consistent with the present Higgs boson data. In contrast the minimal AMSB has a narrower allowed range in $\tan\beta$. These different AMSB scenarios, while consistent with present Higgs boson measurements, can be further tested by future, more precise data in the Higgs sector.

DOI: 10.1103/PhysRevD.87.115020 PACS numbers: 12.60.Jv, 14.80.Da, 95.35.+d

I. INTRODUCTION

The ATLAS and CMS experiments at the Large Hadron Collider (LHC) have reported the discovery of a new boson compatible with the Standard Model (SM) Higgs in July 2012 [1,2], and updated results of the measurements of the Higgs couplings with more precision have been recently released (Refs. [3–15]). All the results are compatible with the predictions for an SM Higgs boson with a mass of about 126 GeV. This discovery is especially important in the context of new physics models, and in particular supersymmetry (SUSY), where the Higgs mass and decay rates can be related to the SUSY parameters.

In this paper, we consider specific scenarios in which anomaly mediation supersymmetry-breaking mechanisms are assumed. In particular, we discuss the implications of B-physics data, LHC Higgs measurements and cold dark matter relic abundance. We discuss different possibilities, such as minimal anomaly mediation (mAMSB) [16,17], hypercharged anomaly mediation (HC-AMSB) [18] and mixed moduli-anomaly mediation (MM-AMSB) [19]. Anomaly mediation models in relation with dark matter and cosmology were also discussed in Ref. [20].

Anomaly mediation supersymmetry-breaking (AMSB) models are based on the fact that the conformal anomaly gives a general and model-independent contribution to gaugino masses which is always present and which can be the dominant contribution when there is no direct tree-level coupling which transfers the SUSY breaking from the hidden sector to the observable sector. This contrasts with the mSUGRA mechanism which is based on the existence of specific tree-level terms. These models are theoretically very appealing as based on existing forces (gravity) and on well-motivated string theory ideas. A well-known problem however in the AMSB scenario is the presence of tachyonic sleptons. This problem can be solved assuming the presence of an intermediate threshold scale. Different supersymmetry-breaking scenarios can be obtained starting from this framework, such as mAMSB, HC-AMSB and MM-AMSB, which we briefly review in the following. It is quite remarkable that present data from different sectors and in particular the recent LHC results for the Higgs boson are able to partially constrain the parameter space of these models. We discuss in the following the implications of such data and the interplay with other constraints coming principally from B-physics and dark matter relic abundance.

This paper is organized as follows. In Sec. II we discuss briefly the theoretical framework of the different anomaly-mediated supersymmetry-breaking setups. In Sec. III the implications of the flavor physics and relic-density constraints are presented, as well as the Higgs mass constraints

*alexandre.arbey@ens-lyon.fr
†deandrea@ipnl.in2p3.fr
‡mahmoudi@in2p3.fr
§tarhini@ipnl.in2p3.fr

and the possibilities to obtain branching ratios for the light *CP*-even Higgs in agreement with the present results at the LHC for the parameter spaces of the different AMSB models. Conclusions are given in Sec. V.

II. THEORETICAL FRAMEWORK

A. mAMSB

The mAMSB scenario can be described both from a higher-dimensional spacetime point of view [16], where the SUSY breaking occurs on a separate brane and is communicated to the visible sector via the super-Weyl anomaly, or from a four-dimensional perspective [17], where a model-independent contribution to the gaugino mass is obtained from the conformal anomaly. In models without singlets this mechanism is the dominant one in the gaugino mass. The soft SUSY-breaking terms can be calculated in terms of a single parameter, the gravitino mass $m_{3/2}$. Nonetheless, as an attempt to avoid the tachyonic slepton problem, it is assumed that the scalar particles have a universal mass m_0 at the Grand Unified Theory scale, which leads to positive AMSB soft SUSY-breaking terms. The mAMSB model possesses only four parameters,

$$m_0,\ m_{3/2},\ \tan\beta,\ \mathrm{sign}(\mu). \tag{1}$$

The soft SUSY-breaking gaugino mass terms are related to $m_{3/2}$ by [21]

$$M_i = \frac{\beta_i}{g_i} m_{3/2}, \tag{2}$$

where $i = 1 \ldots 3$, g_i are the coupling constants and β_i the corresponding β functions. The soft SUSY-breaking sfermion mass terms and fermion trilinear couplings are given by

$$m_{\tilde{f}}^2 = -\frac{1}{4}\left(\sum_{i=1}^{3}\frac{d\gamma}{dg_i}\beta_i + \frac{d\gamma}{dy_f}\beta_f\right)m_{3/2}^2 + m_0^2, \tag{3}$$

$$A_f = \frac{\beta_f}{y_f} m_{3/2}, \tag{4}$$

where β_f is the β function corresponding to the Yukawa coupling y_f and $\gamma = \partial \ln Z/\partial \ln \mu$, where Z is the wave-function renormalization constant.

B. HC-AMSB

A substitute approach to solve the tachyonic lepton problem is the HC-AMSB scenario [18]. In this model, the minimal supersymmetric Standard Model (MSSM) is bound to a D-brane and a geometrically separated hidden sector generates a hypercharge gaugino mass [22]. Therefore, the tachyon problem can be solved by an increase in the slepton masses which results from an additional contribution to the gaugino mass M_1. We parametrize the HC-AMSB symmetry breaking using a dimensionless quantity α which determines the hypercharge contribution relative to the soft bino mass term in AMSB.

The HC-AMSB scenario also has four parameters,

$$\alpha = \frac{\tilde{M}_1}{m_{3/2}},\ m_{3/2},\ \tan\beta,\ \mathrm{sgn}(\mu), \tag{5}$$

where $\tilde{M}_1$ is the additional hypercharge contribution to M_1.

The anomaly mediation and hypercharge mediation have a common theoretical setup, and the two types of mediation are able to compensate the phenomenological shortcomings of each other, giving rise to a realistic and well-motivated model. Indeed the minimal AMSB model predicts a negative mass squared for the sleptons (and prefers heavy squarks) while the pure hypercharge mediation suffers from negative squared masses for stops and sbottoms (and prefers heavy sleptons). Combining the hypercharge and anomaly mediation setups gives rise to a phenomenologically viable spectra in a sizeable range of the parameter space of the model.

In the HC-AMSB model, the soft SUSY-breaking terms are identical to the AMSB ones, apart from the bino and fermion mass terms [21],

$$M_1 = \left(\alpha + \frac{\beta_1}{g_1}\right)m_{3/2}, \tag{6}$$

$$m_{\tilde{f}}^2 = -\frac{1}{4}\left(\sum_{i=1}^{3}\frac{d\gamma}{dg_i}\beta_i + \frac{d\gamma}{dy_f}\beta_f\right)m_{3/2}^2. \tag{7}$$

At the two-loop level, the other gaugino masses, M_2 and M_3, receive a contribution from the bino mass term [22].

C. MM-AMSB

The MM-AMSB scenario [19] can be used as a third possibility to solve the tachyon problem. It is based on type-IIB superstrings with stabilized moduli [23]. In this model, the moduli fields which describe the extra dimensions and the Weyl anomaly have comparable contributions to the SUSY breaking in the observable sector. The spatial extra dimensions are compactified with flux which minimizes the potential of moduli and represents a starting point to find the fundamental state which leads to MSSM at low energy [23]. The soft SUSY-breaking terms receive contributions of comparable magnitude from both the anomaly and modulus, which can increase the slepton masses and solve the tachyon problem. The MM-AMSB scenario has four parameters,

$$\alpha,\ m_{3/2},\ \tan\beta,\ \mathrm{sgn}(\mu), \tag{8}$$

where α parametrizes the relative contributions of modulus mediation and anomaly mediation to the soft breaking terms. A large α corresponds to a mediation from the moduli, and a small α to a mediation from the anomaly. Indeed in the limit where $\alpha \to 0$, we obtain pure AMSB soft SUSY-breaking terms with a negative squared mass for

the sleptons. For intermediate values of α which are more interesting for our studies, the problem of tachyonic sleptons is absent [19]. The mass scale of supersymmetry-breaking parameters is given by the gravitino mass $m_{3/2}$. The soft SUSY parameters are given by [23]

$$M_i = \left(\frac{\alpha}{16\pi^2} + \frac{\beta_i}{g_i}\right) m_{3/2},$$
$$m_{\tilde{f}}^2 = \left\{\frac{\alpha^2}{256\pi^4} + \frac{\alpha}{4\pi^2}\xi_f - \frac{1}{4}\left(\sum_{i=1}^{3}\frac{d\gamma}{dg_i}\beta_i + \frac{d\gamma}{dy_f}\beta_f\right)\right\} m_{3/2}^2,$$
$$A_f = \left(-\frac{3\alpha}{16\pi^2} + \frac{\beta_f}{y_f}\right) m_{3/2}, \tag{9}$$

with

$$\xi_f = \frac{3}{4}y_f^2 - \sum_a g_a^2 C_2^a(f), \tag{10}$$

where C_2^a and g_a are the quadratic Casimir and coupling of the ath gauge group corresponding to the sfermion.

III. TOOLS AND CONSTRAINTS

In order to study the different AMSB scenarios, we use ISAJET 7.82 [24] to generate the SUSY spectra, compute the flavor observables and relic density with SUPERISO RELIC V3.2 [25,26], and we calculate the Higgs branching fractions and decay widths with HDECAY 5.11 [27]. In the following, we disregard the case of negative sign(μ) since it is disfavored by the muon anomalous magnetic moment constraint, when assuming that supersymmetric contributions fill the gap between the measurements and the SM predictions (typically squarks are assumed heavy to explain the Higgs boson mass and LHC bounds, while sleptons, neutralinos and charginos may be light to be consistent with the $g-2$ muon results; see Ref. [28] for a recent analysis). Also, we impose the condition on the SUSY-breaking scale $M_S = \sqrt{m_{\tilde{t}_1} m_{\tilde{t}_2}} < 3$ TeV as a typical scale to limit fine-tuning.

A. Flavor bounds

It is well known that flavor-physics observables provide important indirect constraints on the MSSM as they are sensitive to the SUSY parameters through virtual corrections. Similar considerations apply also in the case of the models under study.

We first consider the inclusive branching ratio of $B \to X_s\gamma$. This decay has been thoroughly studied in the literature as its SM contributions only appear at loop level. The theoretical uncertainties as well as the experimental errors are also very well under control. The $B \to X_s\gamma$ branching ratio is particularly constraining in the large-$\tan\beta$ region where it receives large corrections from the SUSY loops. We use the following interval at 95% C.L.:

$$2.63 \times 10^{-4} < \mathrm{BR}(B \to X_s\gamma) < 4.23 \times 10^{-4}, \tag{11}$$

which is obtained using the latest experimental world average from the Heavy Flavor Averaging Group of $(3.43 \pm 0.21 \pm 0.07) \times 10^{-4}$ [29], after taking into account the theoretical and experimental errors [25,30].

Another important observable in constraining SUSY parameters is the branching ratio of $B_s \to \mu^+\mu^-$, which is also a loop-level observable and suffers from helicity suppression in the SM. In SUSY it can receive extremely large enhancements by several orders of magnitude at large $\tan\beta$. The first evidence for this decay has been reported by the LHCb collaboration very recently [31]. We use the following 95% C.L. interval which includes 10% theoretical error [32]:

$$0.99 \times 10^{-9} < \mathrm{BR}(B_s \to \mu^+\mu^-)_{\mathrm{untag}} < 6.47 \times 10^{-9}, \tag{12}$$

where "untag" denotes the untagged branching fraction, which can be derived from the CP-averaged branching fraction and directly compared to the experimental measurement [33–35].

The purely leptonic decay of $B_u \to \tau\nu$ on the other hand is sensitive to supersymmetry through the exchange of a charged Higgs boson already at tree level, which does not suffer from the helicity suppression of the SM contribution with the exchange of a W boson. This decay can therefore provide stringent constraints. The combination of the most recent Belle and *BABAR* results gives $(1.14 \pm 0.23) \times 10^{-4}$ [36,37] which, including the theoretical errors, leads to the following allowed interval:

$$0.40 \times 10^{-4} < \mathrm{BR}(B_u \to \tau\nu) < 1.88 \times 10^{-4}. \tag{13}$$

We used $f_B = 194 \pm 10$ MeV [32] and $V_{ub} = (4.15 \pm 0.49) \times 10^{-3}$ [38] for the calculation of this branching ratio.

Other flavor observables could be added to this list; however, we have just included the most stringent ones for this analysis. A more complete analysis including all flavor information requires in principle a global fit to all observables, similar to the ones performed to test the Standard Model. This however goes beyond the scope of this preliminary screening of the extensions of AMSB models discussed here.

B. Relic density

The WMAP data [39] provide precise observations of the cold dark matter density in the Universe. We use them to impose constraints on the AMSB parameter spaces by computing the relic density with SUPERISO RELIC. We consider the WMAP interval at 95% C.L. increased by 10% of theoretical error [40,41] to account for the uncertainties in the calculation of the relic density,

$$0.068 < \Omega_\chi h^2 < 0.155. \tag{14}$$

However the relic density constraint can be falsified in an alternative cosmological model [42] or if dark matter is composed of more than one species (with e.g., moduli [43], axions or axinos [44,45]) and we therefore also consider a loose interval,

$$10^{-4} < \Omega_\chi h^2 < 0.155, \tag{15}$$

in which we relaxed the lower bound.

In addition to these bounds, we impose the neutralino to be the lightest supersymmetric particle (LSP) to avoid the cosmological problems related to charged or not-so-weakly-interacting relics.

C. Higgs searches

The discovery of a Higgs-like particle at the LHC provides important information on the MSSM [46–68]. In the following, we associate the newly discovered boson to the lightest *CP*-even Higgs h. The Higgs mass value close to 126 GeV imposes constraints on the parameter space of supersymmetric models which enter the radiative corrections. The leading part of these corrections arises from the top/stop loops,

$$(\Delta M_h^2)_{\tilde{t}} \approx \frac{3G_F}{\sqrt{2}\pi^2} m_t^4 \left[-\ln\left(\frac{m_{\tilde{t}}^2}{M_S^2}\right) + \frac{X_t^2}{M_S^2}\left(1 - \frac{X_t^2}{12M_S^2}\right)\right], \tag{16}$$

where $M_S = \sqrt{m_{\tilde{t}_1} m_{\tilde{t}_2}}$ and $X_t = A_t - \mu/\tan\beta$ is the stop mixing parameter. This correction is maximized for $|X_t| = \sqrt{6}M_S$, which is referred to as the "maximal mixing" scenario, and minimized for $X_t = 0$ in the "minimal mixing" scenario. The "typical mixing" scenario corresponds to the intermediate values of $|X_t| \approx M_S$.

In the figures, the constraint on the Higgs boson mass will be taken at the two-sigma level, $121.5 < M_h < 129.9$ GeV. The extra information provided by the measurements of Higgs branching ratios provides extra useful constraints. The latest LHC measurements of the Higgs mass and decay rates are summarized in Table I. We use in the following the by now standard notation of signal strengths normalized to the SM expectation, defined as

TABLE I. Experimental average for the Higgs mass and rates [69].

	Value	Experiment
M_h	125.7 ± 2.1 GeV	ATLAS [9], CMS [10]
$\mu_{\gamma\gamma}$	1.20 ± 0.30	ATLAS [11], CMS [12]
μ_{ZZ}	1.10 ± 0.22	ATLAS [13], CMS [10]
μ_{WW}	0.77 ± 0.21	ATLAS [14], CMS [15]
$\mu_{b\bar{b}}$	1.12 ± 0.45	ATLAS [70], CMS [71], CDF,D0 [72]
$\mu_{\tau\tau}$	1.01 ± 0.36	ATLAS [70], CMS [73]

$$\mu_{\gamma\gamma,VV} = \frac{\sigma(\text{gluon fusion})}{\sigma_{\text{SM}}(\text{gluon fusion})} \frac{\text{BR}(h \to \gamma\gamma, VV)}{\text{BR}_{\text{SM}}(H \to \gamma\gamma, VV)}, \tag{17}$$

$$\mu_{\tau\tau} = \frac{\sigma(\text{VBF})}{\sigma_{\text{SM}}(\text{VBF})} \frac{\text{BR}(h \to \tau\tau)}{\text{BR}_{\text{SM}}(H \to \tau\tau)}, \tag{18}$$

$$\mu_{b\bar{b}} = \frac{\sigma(\text{HV})}{\sigma_{\text{SM}}(\text{HV})} \frac{\text{BR}(h \to b\bar{b})}{\text{BR}_{\text{SM}}(H \to b\bar{b})}, \tag{19}$$

where VV refers to vector boson ZZ or WW production, and VBF and HV stand for vector boson fusion and associated Higgs vector boson production. For the $\mu_{\gamma\gamma}$ signal strength note that we use the average from ATLAS and CMS as a guideline, but this should be taken with some care as the two experiments have quite different central values; ATLAS has $\mu_{\gamma\gamma} = 1.65^{+0.34}_{-0.30}$ while CMS reports 0.78 ± 0.27. Hereafter, we do not show the constraints from μ_{ZZ}, as they are very similar to the ones from the WW channel.

To evaluate the Higgs production cross sections normalized to the SM values, we use

$$\frac{\sigma(\text{gluon fusion})}{\sigma_{\text{SM}}(\text{gluon fusion})} \approx \frac{\Gamma^h}{\Gamma^H_{\text{SM}}} \frac{\text{BR}(h \to gg)}{\text{BR}_{\text{SM}}(H \to gg)}, \tag{20}$$

$$\frac{\sigma(\text{VBF})}{\sigma_{\text{SM}}(\text{VBF})} \approx \frac{\sigma(\text{HV})}{\sigma_{\text{SM}}(\text{HV})} \approx \frac{\Gamma^h}{\Gamma^H_{\text{SM}}} \frac{\text{BR}(h \to VV)}{\text{BR}_{\text{SM}}(H \to VV)}, \tag{21}$$

where Γ^h and Γ^H_{SM} are respectively the MSSM h and SM H total decay widths.

In the following, we do not impose strict intervals on the calculated signal strengths, but we comment on the compatibility of the results with the experimental data.

IV. RESULTS

We consider the constraints from flavor physics, dark matter and LHC Higgs searches in the context of minimal AMSB, hypercharge AMSB and mixed-moduli AMSB. We show in the following how the available parameter space is reduced in these different models when applying the available constraints.

A. mAMSB

To study the mAMSB scenario, we perform flat scans by varying the parameters in the following ranges:

$$\begin{aligned} m_0 &\in [50, 10000] \text{ GeV}, \\ m_{3/2} &\in [0, 500] \text{ TeV}, \\ \tan\beta &\in [1, 55], \end{aligned} \tag{22}$$

and use a sample of more than 1 million points. We first consider the constraints obtained from the Higgs mass measurement. In Fig. 1, we present the light *CP*-even

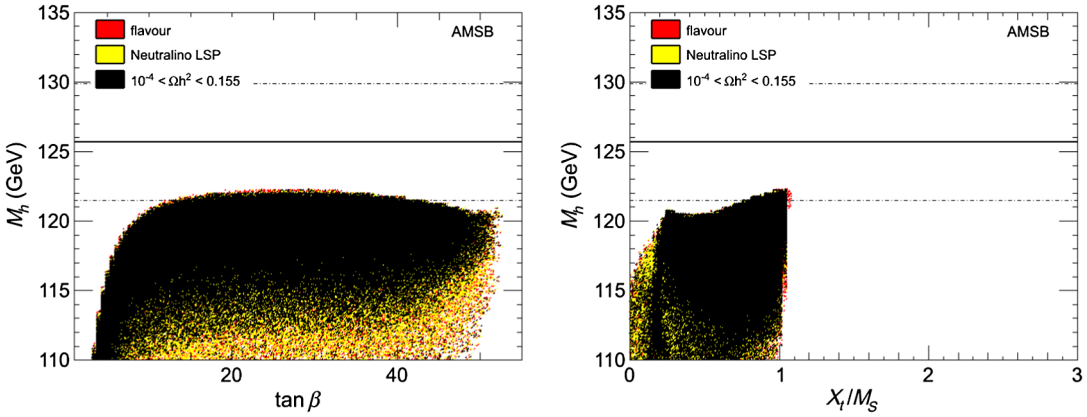

FIG. 1 (color online). Light Higgs mass as functions of tan β (left panel) and X_t/M_S (right panel) in mAMSB. The red points are all points compatible with the constraints from flavor physics described in Sec. III A. The yellow points also have a neutralino LSP. The black points are in addition consistent with the upper bound of the relic density constraint. The horizontal solid line corresponds to the central value of the Higgs mass and the dashed lines to the 2σ deviations.

Higgs mass as a function of tan β and X_t/M_S, and show the points *compatible* with the flavor and relic density constraints. First, we see that M_h is limited to values below 122 GeV. The reason for this behavior is related to the fact that in the mAMSB scenario, X_t/M_S is small, corresponding to a no-mixing regime which leads to a lower Higgs mass. Second, no mAMSB point is compatible with the tight relic density interval of Eq. (14), but there exist points compatible with the loose relic density interval of Eq. (15). One of the limiting factors for the light CP-even Higgs mass comes from the restriction $M_S < 3$ TeV that we impose to limit fine-tuning. We have checked our results for the Higgs mass numerically using four generators: ISAJET [24], SOFTSUSY [74], SUSPECT [75] and SPHENO [76]. While the results from the first three generators are fully consistent, the results of SPHENO were different and this may explain the different result found in Ref. [77]. Our result is consistent with the one in Ref. [68].

We consider now the Higgs signal strengths in Fig. 2 as a function of tan β. We include the 2σ constraint from the Higgs mass in the plots. We first notice that most of the valid points are close to the SM values of the Higgs strengths. Concerning the $\mu_{\gamma\gamma}$ signal strength, ATLAS and CMS have different central values—as indicated after Table I—and even if at present the average of the two values can be used as just a rough guideline, future, more precise measurements are important for this class of models as values close to the SM results are favorable, while values larger than one are clearly disfavored in these scenarios. Moreover, all the Higgs strengths can be decreased, which corresponds to a suppression in the production cross sections. In particular for the Higgs to diphoton decay, the predicted strength already stands below the 2σ experimental lower bound. We see however that points not compatible with the cosmology constraints can have an increased signal in $\gamma\gamma$ for tan $\beta \sim 20$. However, all these points correspond to a scenario in which the LSP is a stau, and the increase is induced by light stau loops as described in Ref. [78]. Nevertheless, scenarios with a charged LSP are strongly disfavored by the cosmology requirements for a neutral dark matter stable particle. As a consequence, the mAMSB scenario is compatible with the Higgs mass measurements only marginally at the two-sigma level since the maximum attainable Higgs mass is below 122 GeV, and also the relic abundance constraint can only be met with the loose bounds described above.

B. HC-AMSB

The HC-AMSB scenario provides a modification of the M_1 bino mass, as discussed in Sec. II B. We have generated a sample of more than 1 million points through flat scans over the parameters in the following intervals:

$$\begin{aligned} \alpha &\in [-0.3, 0.3], \\ m_{3/2} &\in [0, 500] \text{ TeV}, \\ \tan\beta &\in [1, 55]. \end{aligned} \tag{23}$$

In Fig. 3, we plot the light Higgs mass as functions of tan β and X_t/M_S. Contrary to the mAMSB scenario, the Higgs mass can reach 126 GeV and therefore be fully consistent with the mass constraint. The sfermions are lighter in this scenario as compared to in the mAMSB scenario, as can be seen by comparing Eqs. (3) and (7)which differ by a term m_0^2. Numerically, as m_0 can typically be in the TeV range, the sfermion masses in the HC-AMSB scenario are typically lighter by the same amount with respect to the corresponding sfermions in the mAMSB model. Moreover X_t/M_S can reach larger values. On the other hand, no point in this scenario is at the same time consistent with the tight relic-density constraint of Eq. (14), but many points fulfill both the Higgs and loose relic-density bounds. More specifically, the allowed points have tan $\beta \gtrsim 5$ and $X_t \gtrsim M_S$,

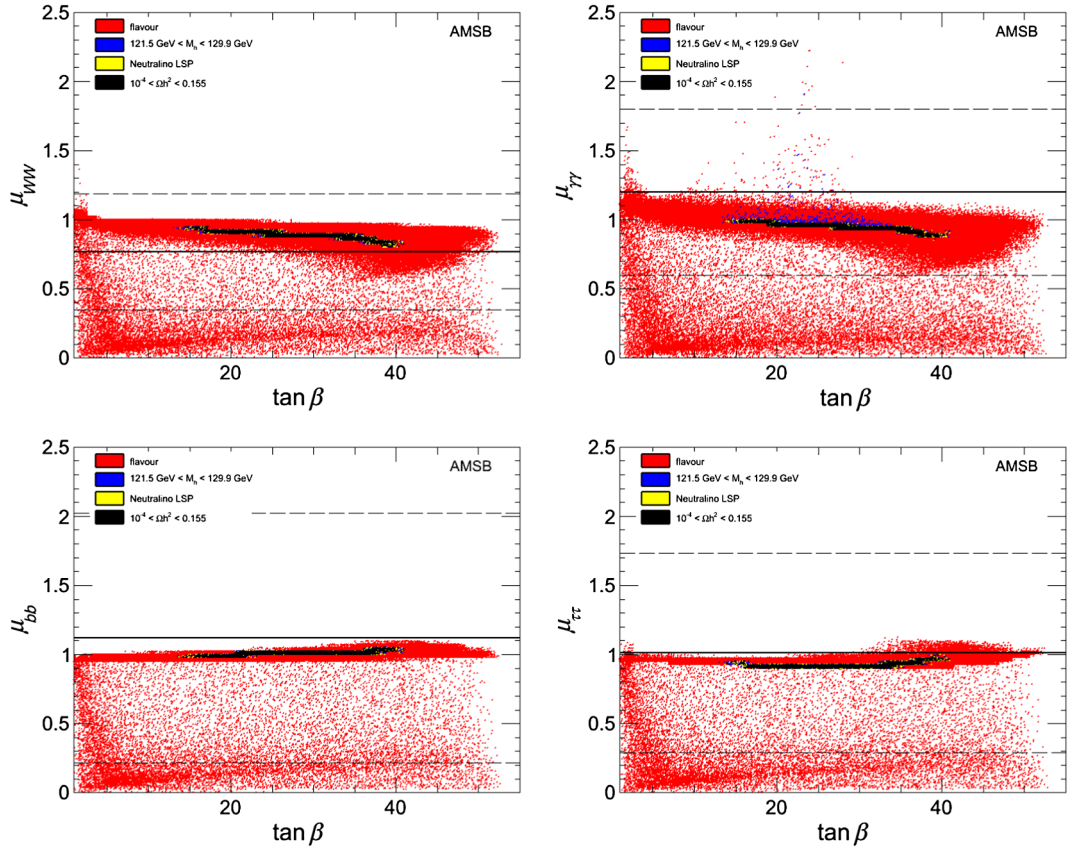

FIG. 2 (color online). μ_{WW} (upper left), $\mu_{\gamma\gamma}$ (upper right), $\mu_{b\bar{b}}$ (lower left) and $\mu_{\tau\tau}$ (lower right) as functions of $\tan\beta$ in the mAMSB model. The red points are favored by the flavor-physics constraints, the blue points are compatible with the Higgs mass constraint, the yellow points have a neutralino LSP and the black points in addition are compatible with the upper bound of the relic density constraint. The yellow and blue regions almost coincide with the black one, so most yellow and blue points are masked by the black region. The horizontal solid lines correspond to the experimental central values given in Table I and the dashed lines to the 2σ intervals.

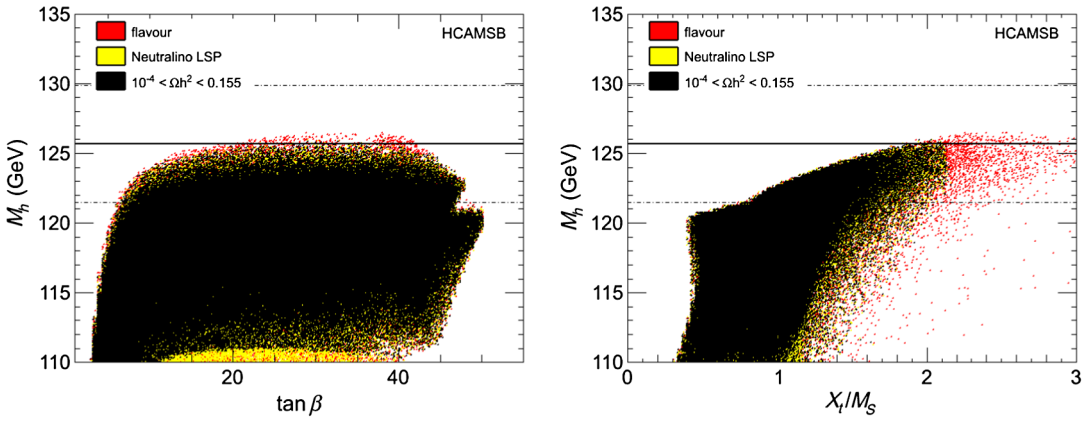

FIG. 3 (color online). Light Higgs mass as functions of $\tan\beta$ (left panel) and X_t/M_S (right panel) in HC-AMSB. The red points are all points compatible with the constraints from flavor physics described in Sec. III A, the yellow points have a neutralino LSP and the black points are in addition consistent with the upper bound of the relic density constraint. The horizontal solid line corresponds to the central value of the Higgs mass and the dashed lines to the 2σ deviations.

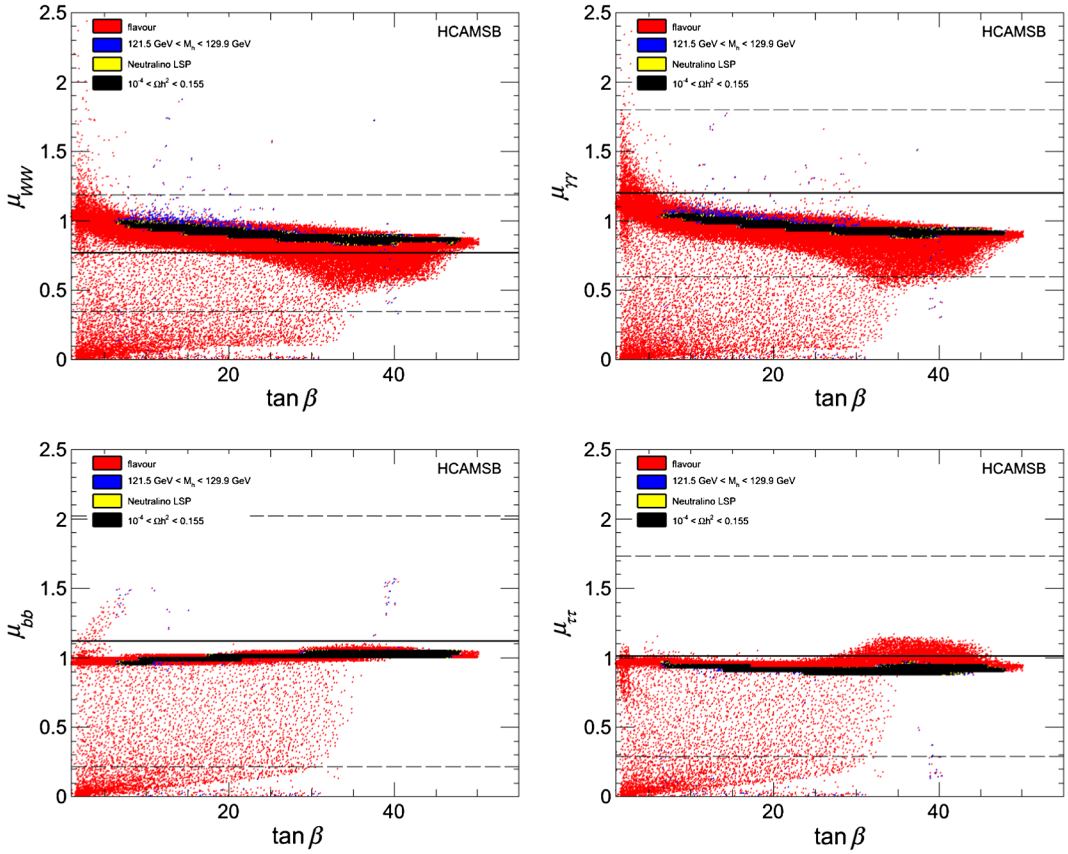

FIG. 4 (color online). μ_{WW} (upper left), $\mu_{\gamma\gamma}$ (upper right), $\mu_{b\bar{b}}$ (lower left) and $\mu_{\tau\tau}$ (lower right) as functions of $\tan\beta$ in the HC-AMSB model. The red points are favored by the flavor-physics constraints, the blue points are compatible with the Higgs mass constraint, the yellow points have a neutralino LSP and the black points in addition are compatible with the upper bound of the relic density constraint. The horizontal solid lines correspond to the experimental central values given in Table I and the dashed lines to the 2σ intervals.

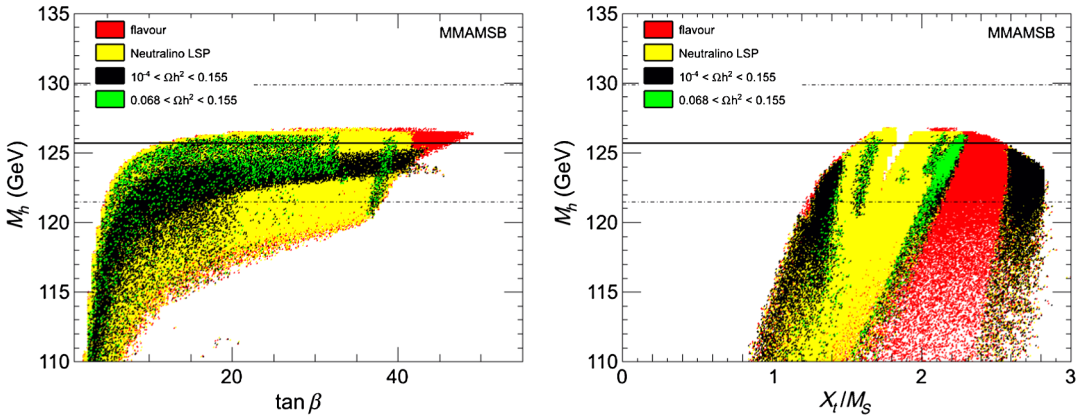

FIG. 5 (color online). Light Higgs mass as functions of $\tan\beta$ (left panel) and X_t/M_S (right panel) in MM-AMSB. The red points are all points compatible with the constraints from flavor physics described in Sec. III A. The yellow points have also a neutralino LSP. The black points are consistent with the loose relic density constraint of Eq. (15). The green points are in addition consistent with the tight relic density constraint given in Eq. (14). The horizontal solid line corresponds to the central value of the Higgs mass and the dashed lines to the 2σ deviations.

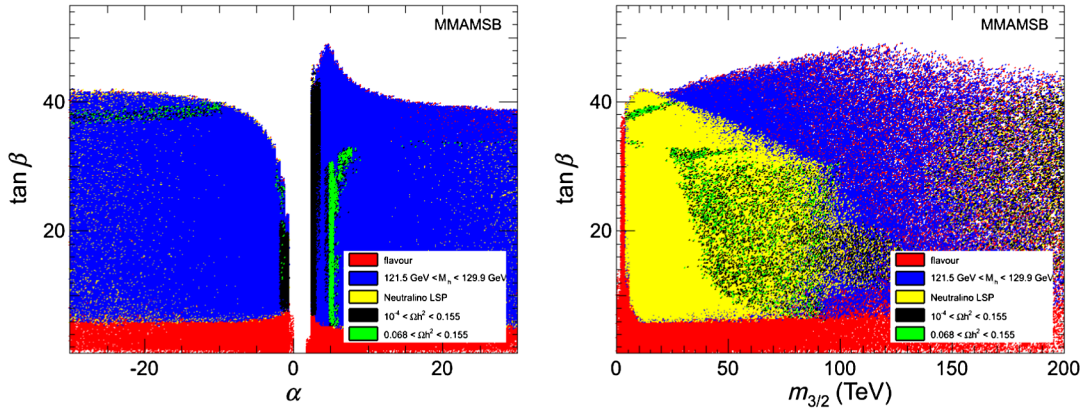

FIG. 6 (color online). Constraints from flavor physics, Higgs mass and relic density in the $(\alpha, \tan\beta)$ (left panel) and $(m_{3/2}, \tan\beta)$ (right panel) parameter planes in the MM-AMSB model. The red points are favored by the flavor-physics constraints, the blue points are compatible with the Higgs mass constraint, the yellow points have a neutralino LSP, the black points are compatible with the loose relic density constraint and the green points are in addition compatible with the tight relic-density constraint.

and therefore correspond to the typical- or maximal-mixing regimes.

In Fig. 4, we consider the μ_{WW}, $\mu_{\gamma\gamma}$, $\mu_{b\bar{b}}$ and $\mu_{\tau\tau}$ signal strengths of the Higgs as a function of $\tan\beta$. First, the bulk of points compatible with the flavor constraints are consistent with the SM signal strengths. When imposing the Higgs mass constraint, $\tan\beta$ is restricted to large values, as already noticed in Fig. 3, and most of the points with low

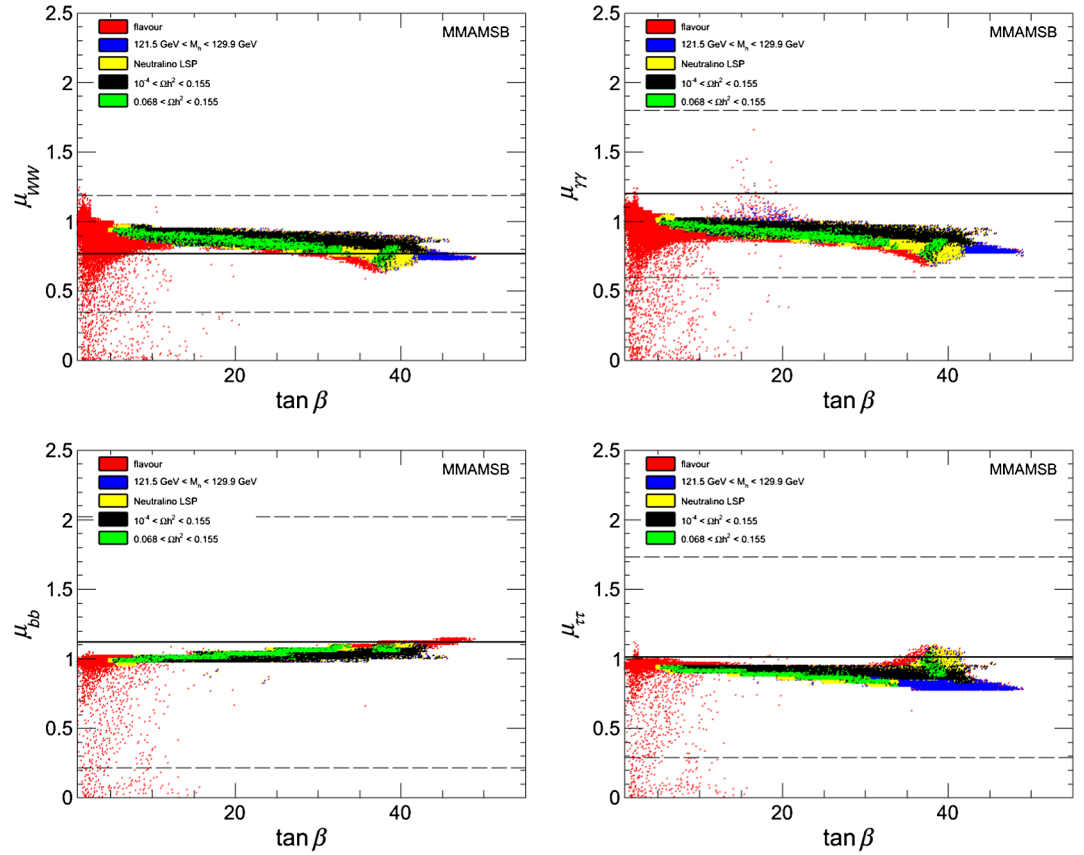

FIG. 7 (color online). μ_{WW} (upper left), $\mu_{\gamma\gamma}$ (upper right), $\mu_{b\bar{b}}$ (lower left) and $\mu_{\tau\tau}$ (lower right) as functions of $\tan\beta$ in the MM-AMSB model. The red points are favored by the flavor-physics constraints, the blue points are compatible with the Higgs mass constraint, the yellow points have a neutralino LSP, the black points are compatible with the loose relic-density constraint and the green points in addition are compatible with the tight relic-density constraint. The horizontal solid lines correspond to the experimental central values given in Table I and the dashed lines to the 2σ intervals.

signal strengths are removed. Finally, we impose the neutralino LSP and loose relic-density constraints, and note that this requirement removes points with enhanced $\gamma\gamma$ signal strength. While this scenario is well compatible with the latest Higgs search results, it may be disfavored in the future if the $\gamma\gamma$ signal strength value is confirmed to be larger than the SM value. Thus, the HC-AMSB model can explain simultaneously flavor physics, loose relic-density bounds and the current Higgs search results, but can be challenged by future, more precise data.

C. MM-AMSB

As we already showed in Ref. [20], the MM-AMSB has the advantage of providing solutions consistent with the tight relic-density constraint. We here compare this model to the latest Higgs constraints. To study this scenario, we vary the parameters in the following ranges:

$$\begin{aligned} \alpha &\in [-30, 30], \\ m_{3/2} &\in [0, 500] \text{ TeV}, \\ \tan\beta &\in [1, 55], \end{aligned} \tag{24}$$

using flat scans generating more than 1 million points.

In Fig. 5, we plot the light Higgs mass as functions of $\tan\beta$ and X_t/M_S. As for the HC-AMSB scenario, the Higgs mass can reach 126 GeV, in a region corresponding to the typical- and maximal-mixing regimes in the stop sector. In this scenario, both the sfermion masses and trilinear couplings are modified by the modulus mediation. We note that imposing the lower bound of the relic density constraint makes apparent two distinct regions of compatibility: a large one with $\tan\beta \lesssim 30$ and $X_t/M_S \gtrsim 1-2$ corresponding to a typical mixing, and a narrow strip around $\tan\beta \sim 37$ and $X_t \gtrsim 2M_S$ corresponding to a maximal mixing. In Fig. 6 we consider the effects of the constraints in the $(\alpha, \tan\beta)$ and $(m_{3/2}, \tan\beta)$ parameter planes. We see clearly the difference between the two regions highlighted in Fig. 5: the low-$\tan\beta$ region has positive values of α typically around 6, while the $\tan\beta \sim 37$ strip corresponds to negative α and small $m_{3/2}$. In terms of physical spectra, in both scenarios the neutralino is relatively heavy ($\gtrsim$500 GeV). The negative α region corresponds to Higgs resonances, with a bino-like neutralino 1 mass approximately half the H and A Higgs masses, while the positive α region has stau and stop masses close to the neutralino mass, resulting in important coannihilations, and the neutralino 1 is a mixed bino-wino state.

In Fig. 7, we consider the μ_{WW}, $\mu_{\gamma\gamma}$, $\mu_{b\bar{b}}$ and $\mu_{\tau\tau}$ signal strengths of the Higgs as a function of $\tan\beta$. In comparison with the other AMSB scenarios, we find for the MM-AMSB model a situation similar to the one of the HC-AMSB model, where the Higgs mass constraint is satisfied: the signal strength for the decay of the Higgs boson to two photons is consistent with the preferred dark matter region of the parameter space within two sigmas.

V. CONCLUSIONS

Anomaly mediation and its extensions, including hypercharge and moduli for supersymmetry breaking, are attractive models from the theoretical point of view. The well-known shortcomings of these models have been largely discussed and corrected in the literature. However detailed phenomenological implications of the recent dark matter, Higgs, flavor and collider data were not yet considered. In this paper we have discussed these limits, taking into account the most important recent flavor and Higgs search results, together with the dark matter constraints in order to establish which among these models are still compatible with data.

The minimal AMSB model is consistent with the loose relic density dark matter constraints, but consistency is only marginal at the two-sigma level, especially due to the Higgs mass constraint. We therefore consider this minimal scenario much less attractive, once the phenomenological constraints are imposed.

Concerning the HC-AMSB model, it is consistent with the loose relic density dark matter constraints and with the Higgs mass value. Relaxing the neutralino LSP requirement and the relic density constraints allows for points with increased $\mu_{\gamma\gamma}$ in the region of light stau masses. This scenario with light staus has been thoroughly studied in the literature; however, in the HC-AMSB scenario it corresponds to a region in which the stau is the LSP, making it inconsistent with cosmology. Contrary to the mAMSB and the HC-AMSB, the MM-AMSB model provides solutions compatible with flavor, collider data and the full relic-density constraint. Therefore, the MM- and, to a lesser extent, the HC-AMSB model, are still attractive solutions of supersymmetry breaking which are consistent with present data. Future improvements in the precision of the Higgs mass measurements may easily rule out the minimal AMSB model if the present central value is confirmed. The MM- and HC-AMSB models will still be consistent in that case, but further constraints can be obtained from more precise determinations of the signal strength in the measured decay channels. In particular for the $\mu_{\gamma\gamma}$ signal strength, ATLAS and CMS have currently quite different central values, as indicated after Table I. At present the average of the two values can be used as just a rough guideline. This shows the importance of present and future LHC data, in combination with flavor and dark matter constraints to suggest the path to be followed in the investigation of physics beyond the Standard Model.

ACKNOWLEDGMENTS

We acknowledge partial support from the Labex-LIO (Lyon Institute of Origins), CF-Theorie IN2P3 and the European Union FP7 ITN INVISIBLES Network (Marie Curie Actions, PITN-GA- 2011-289442). We are also grateful to the Grenoble 125 GeV Higgs workshop where part of this work was carried out.

[1] ATLAS collaboration, Phys. Lett. B **716**, 1 (2012).
[2] CMS collaboration, Phys. Lett. B **716**, 30 (2012).
[3] ATLAS Collaboration, Report No. ATLAS-CONF-2012-160.
[4] ATLAS Collaboration, Report No. ATLAS-CONF-2012-161.
[5] CMS Collaboration, Report No. CMS PAS HIG-2012-043.
[6] CMS Collaboration, Report No. CMS PAS HIG-2012-044.
[7] ATLAS Collaboration, Report No. ATLAS-CONF-2012-168.
[8] ATLAS Collaboration, Report No. ATLAS-CONF-2012-169.
[9] ATLAS Collaboration, Report No. ATLAS-CONF-2013-014.
[10] CMS Collaboration, Report No. CMS PAS HIG-2013-002.
[11] ATLAS Collaboration, Report No. ATLAS-CONF-2013-012.
[12] CMS Collaboration, Report No. CMS PAS HIG-2013-001.
[13] ATLAS Collaboration, Report No. ATLAS-CONF-2013-013.
[14] ATLAS Collaboration, Report No. ATLAS-CONF-2013-030.
[15] CMS Collaboration, Report No. CMS PAS HIG-2013-003.
[16] L. Randall and R. Sundrum, Nucl. Phys. **B557**, 79 (1999).
[17] G. F. Giudice, M. A. Luty, H. Murayama, and R. Rattazzi, J. High Energy Phys. 12 (1998) 027; A. Pomarol and R. Rattazzi, J. High Energy Phys. 05 (1999) 013; D. W. Jung and J. Y. Lee, J. High Energy Phys. 03 (2009) 123.
[18] R. Dermisek, H. Verlinde, and L. T. Wang, Phys. Rev. Lett. **100**, 131804 (2008).
[19] K. Choi, K. S. Jeong, and K. I. Okumura, J. High Energy Phys. 09 (2005) 039.
[20] A. Arbey, A. Deandrea, and A. Tarhini, J. High Energy Phys. 05 (2011) 078.
[21] H. Baer, R. Dermisek, S. Rajagopalan, and H. Summy, J. Cosmol. Astropart. Phys. 07 (2010) 014.
[22] H. Baer, R. Dermisek, S. Rajagopalan, and H. Summy, J. High Energy Phys. 10 (2009) 078.
[23] H. Baer, E. K. Park, X. Tata, and T. T. Wang, J. High Energy Phys. 08 (2006) 041.
[24] F. E. Paige, S. D. Protopopescu, H. Baer, and X. Tata, arXiv:hep-ph/0312045.
[25] F. Mahmoudi, Comput. Phys. Commun. **178**, 745 (2008); **180**, 1579 (2009), http://superiso.in2p3.fr.
[26] A. Arbey and F. Mahmoudi, Comput. Phys. Commun. **181**, 1277 (2010), http://superiso.in2p3.fr/relic.
[27] A. Djouadi, J. Kalinowski, and M. Spira, Comput. Phys. Commun. **108**, 56 (1998).
[28] M. Endo, K. Hamaguchi, S. Iwamoto, and T. Yoshinaga, arXiv:1303.4256.
[29] Y. Amhis *et al.* (Heavy Flavor Averaging Group Collaboration), arXiv:1207.1158, and online update at http://www.slac.stanford.edu/xorg/hfag.
[30] F. Mahmoudi, J. High Energy Phys. 12 (2007) 026.
[31] R. Aaij *et al.* (LHCb Collaboration), Phys. Rev. Lett. **110**, 021801 (2013).
[32] F. Mahmoudi, S. Neshatpour, and J. Orloff, J. High Energy Phys. 08 (2012) 092.
[33] S. Descotes-Genon, J. Matias, and J. Virto, Phys. Rev. D **85**, 034010 (2012).
[34] K. De Bruyn, R. Fleischer, R. Knegjens, P. Koppenburg, M. Merk, A. Pellegrino, and N. Tuning, Phys. Rev. Lett. **109**, 041801 (2012); K. De Bruyn, R. Fleischer, R. Knegjens, P. Koppenburg, M. Merk, and N. Tuning, Phys. Rev. D **86**, 014027 (2012).
[35] A. Arbey, M. Battaglia, F. Mahmoudi, and D. Martinez Santos, Phys. Rev. D **87**, 035026 (2013).
[36] I. Adachi *et al.* (Belle Collaboration), Phys. Rev. Lett. **110**, 131801 (2013).
[37] J. P. Lees *et al.* (*BABAR* Collaboration), arXiv:1207.0698.
[38] J. Beringer *et al.* (Particle Data Group Collaboration), Phys. Rev. D **86**, 010001 (2012).
[39] G. Hinshaw *et al.*, arXiv:1212.5226.
[40] M. Hindmarsh and O. Philipsen, Phys. Rev. D **71**, 087302 (2005).
[41] N. Baro, F. Boudjema, and A. Semenov, Phys. Lett. B **660**, 550 (2008).
[42] M. Kamionkowski and M. S. Turner, Phys. Rev. D **42**, 3310 (1990); G. F. Giudice, E. W. Kolb, and A. Riotto, Phys. Rev. D **64**, 023508 (2001); P. Salati, Phys. Lett. B **571**, 121 (2003); G. Gelmini, P. Gondolo, A. Soldatenko, and C. E. Yaguna, Phys. Rev. D **74**, 083514 (2006); A. Arbey and F. Mahmoudi, Phys. Lett. B **669**, 46 (2008); J. High Energy Phys. 05 (2010) 051.
[43] B. S. Acharya, P. Kumar, K. Bobkov, G. Kane, J. Shao, and S. Watson, J. High Energy Phys. 06 (2008) 064.
[44] F. D. Steffen, Eur. Phys. J. C **59**, 557 (2009).
[45] H. Baer, A. Lessa, S. Rajagopalan, and W. Sreethawong, J. Cosmol. Astropart. Phys. 06 (2011) 031.
[46] L. J. Hall, D. Pinner, and J. T. Ruderman, J. High Energy Phys. 04 (2012) 131.
[47] H. Baer, V. Barger, and A. Mustafayev, Phys. Rev. D **85**, 075010 (2012).
[48] S. Heinemeyer, O. Stal, and G. Weiglein, Phys. Lett. B **710**, 201 (2012).
[49] N. D. Christensen, T. Han, and S. Su, Phys. Rev. D **85**, 115018 (2012).
[50] F. Brummer, S. Kraml, and S. Kulkarni, J. High Energy Phys. 08 (2012) 089.
[51] D. Ghosh, M. Guchait, S. Raychaudhuri, and D. Sengupta, Phys. Rev. D **86**, 055007 (2012).
[52] A. Fowlie, M. Kazana, K. Kowalska, S. Munir, L. Roszkowski, E. M. Sessolo, S. Trojanowski, and Y.-L. S. Tsai, Phys. Rev. D **86**, 075010 (2012).
[53] M. W. Cahill-Rowley, J. L. Hewett, A. Ismail, and T. G. Rizzo, Phys. Rev. D **86**, 075015 (2012).
[54] A. Arbey, M. Battaglia, A. Djouadi, and F. Mahmoudi, J. High Energy Phys. 09 (2012) 107.
[55] M. R. Buckley and D. Hooper, Phys. Rev. D **86**, 075008 (2012).
[56] J. Cao, Z. Heng, J. M. Yang, and J. Zhu, J. High Energy Phys. 10 (2012) 079.
[57] S. Antusch, L. Calibbi, V. Maurer, M. Monaco, and M. Spinrath, J. High Energy Phys. 01 (2013) 187.
[58] S. S. AbdusSalam and D. Choudhury, arXiv:1210.3331.
[59] M. W. Cahill-Rowley, J. L. Hewett, A. Ismail, and T. G. Rizzo, arXiv:1211.1981.
[60] W. Altmannshofer, M. Carena, N. R. Shah, and F. Yu, J. High Energy Phys. 01 (2013) 160.
[61] A. Arbey, M. Battaglia, A. Djouadi, and F. Mahmoudi, Phys. Lett. B **720**, 153 (2013).

[62] N. Okada and H. M. Tran, Phys. Rev. D **87**, 035024 (2013).
[63] J. Ellis, F. Luo, K. A. Olive, and P. Sandick, arXiv:1212.4476.
[64] L. E. Ibanez and I. Valenzuela, J. High Energy Phys. 05 (2013) 064.
[65] P. Nath, arXiv:1302.1863.
[66] T. Han, Z. Liu, and A. Natarajan, arXiv:1303.3040.
[67] C. Boehm, P. S. B. Dev, A. Mazumdar, and E. Pukartas, arXiv:1303.5386.
[68] A. Arbey, M. Battaglia, A. Djouadi, F. Mahmoudi, and J. Quevillon, Phys. Lett. B **708**, 162 (2012).
[69] A. Arbey, M. Battaglia, and F. Mahmoudi, arXiv:1303.7450.
[70] ATLAS Collaboration, Report No. ATLAS-CONF-2012-161.
[71] CMS Collaboration, Report No. CMS PAS HIG-2012-044.
[72] T. Aaltonen *et al.* (CDF and D0 Collaborations), Phys. Rev. Lett. **109**, 071804 (2012).
[73] CMS Collaboration, Report No. CMS PAS HIG-2012-004.
[74] B. C. Allanach, Comput. Phys. Commun. **143**, 305 (2002).
[75] A. Djouadi, J. L. Kneur, and G. Moultaka, Comput. Phys. Commun. **176**, 426 (2007).
[76] W. Porod, Comput. Phys. Commun. **153**, 275 (2003).
[77] B. Fuks, B. Herrmann, and M. Klasen, Phys. Rev. D **86**, 015002 (2012).
[78] See e.g., M. Carena, S. Gori, N. R. Shah, C. E. M. Wagner, and L.-T. Wang, J. High Energy Phys. 07 (2012) 175; M. Carena, I. Low, and C. E. M. Wagner, J. High Energy Phys. 08 (2012) 060; G. F. Giudice, P. Paradisi, and A. Strumia, J. High Energy Phys. 10 (2012) 186; U. Haisch and F. Mahmoudi, J. High Energy Phys. 01 (2013) 061.